Received: 22 December 2021 | Revised: 25 February 2022 | Accepted: 9 March 2022

DOI: 10.1002/ar.24919

SPECIAL ISSUE ARTICLE

The Anatomical Record WILEY

Architecture of the bronchial tree in Cuvier's dwarf caiman (*Paleosuchus palpebrosus*)

Emma R. Schachner[1] | **Raul E. Diaz**[2] | **Rob Coke**[3] | **Scott Echols**[4] | **Michelle L. Osborn**[5] | **Brandon P. Hedrick**[1]

[1]Department of Cell Biology and Anatomy, School of Medicine, Louisiana State University Health Sciences Center, New Orleans, Louisiana, USA

[2]Department of Biological Sciences, California State University Los Angeles, Los Angeles, California, USA

[3]San Antonio Zoo, San Antonio, Texas, USA

[4]The Medical Center for Birds, Oakley, California, USA

[5]Department of Comparative Biomedical Sciences, School of Veterinary Medicine, Louisiana State University, Baton Rouge, Louisiana, USA

Correspondence
Emma R. Schachner, Department of Cell Biology & Anatomy, School of Medicine, Louisiana State University Health Sciences Center, New Orleans, Louisiana, USA.
Email: eschachner@gmail.com

Funding information
Division of Electrical, Communications and Cyber Systems, Grant/Award Number: 1541959; Louisiana State University Health Sciences Center Research Enhancement Program Grant

Abstract

We imaged the lungs of five Cuvier's dwarf caiman (*Paleosuchus palpebrosus*) via computed tomography (CT) and micro-computed tomography (μCT) and compared these data to the lungs of the American alligator (*Alligator mississippiensis*). These data demonstrate anatomical commonalities between the lungs of *P. palpebrosus* and *A. mississippiensis*, and a few notable differences. The structural similarities are (a) a proximally narrow, distally widened, hook-shaped primary bronchus; (b) a cervical ventral bronchus that branches of the primary bronchus and immediately makes a hairpin turn toward the apex of the lung; (c) a sequential series of dorsobronchi arising from the primary bronchus caudal to the cervical ventral bronchus; (d) intraspecifically highly variable medial sequence of secondary airways; (e) sac-like laterobronchi; and (f) grossly dead-ended caudal group bronchi in the caudal and ventral aspects of the lung. The primary differences between the two taxa are in the overall number of large bronchi (fewer in *P. palpebrosus*), and the number of branches that contribute to the cardiac regions. Imaging data of both a live and deceased specimen under varying states (postprandial, fasting, total lung capacity, open to atmosphere) indicate that the caudal margin and position of the lungs shift craniocaudally relative to the vertebral column. These imaging data suggest that the smooth thoracic ceiling may be correlated to visceral movement during ventilation, but this hypothesis warrants validation. These results provide the scaffolding for future comparisons between crocodilians, for generating preliminary reconstructions of the ancestral crocodilian bronchial tree, and establishing new hypotheses of bronchial homology across Archosauria.

KEYWORDS

alligator, archosaur, crocodile, evolution, lungs

1 | INTRODUCTION

Avian-like unidirectional airflow patterns have been found in every single extant crocodilian measured (*Alligator mississippiensis*, *Crocodylus niloticus*, *Melanosuchus niger*, *Osteolaemus tetraspis*, *Crocodylus porosus*, *Crocodylus moreletii*, and *Caiman crocodilus*) (Farmer, 2015a, 2015c; Farmer & Sanders, 2010; Schachner et al., 2013), and yet

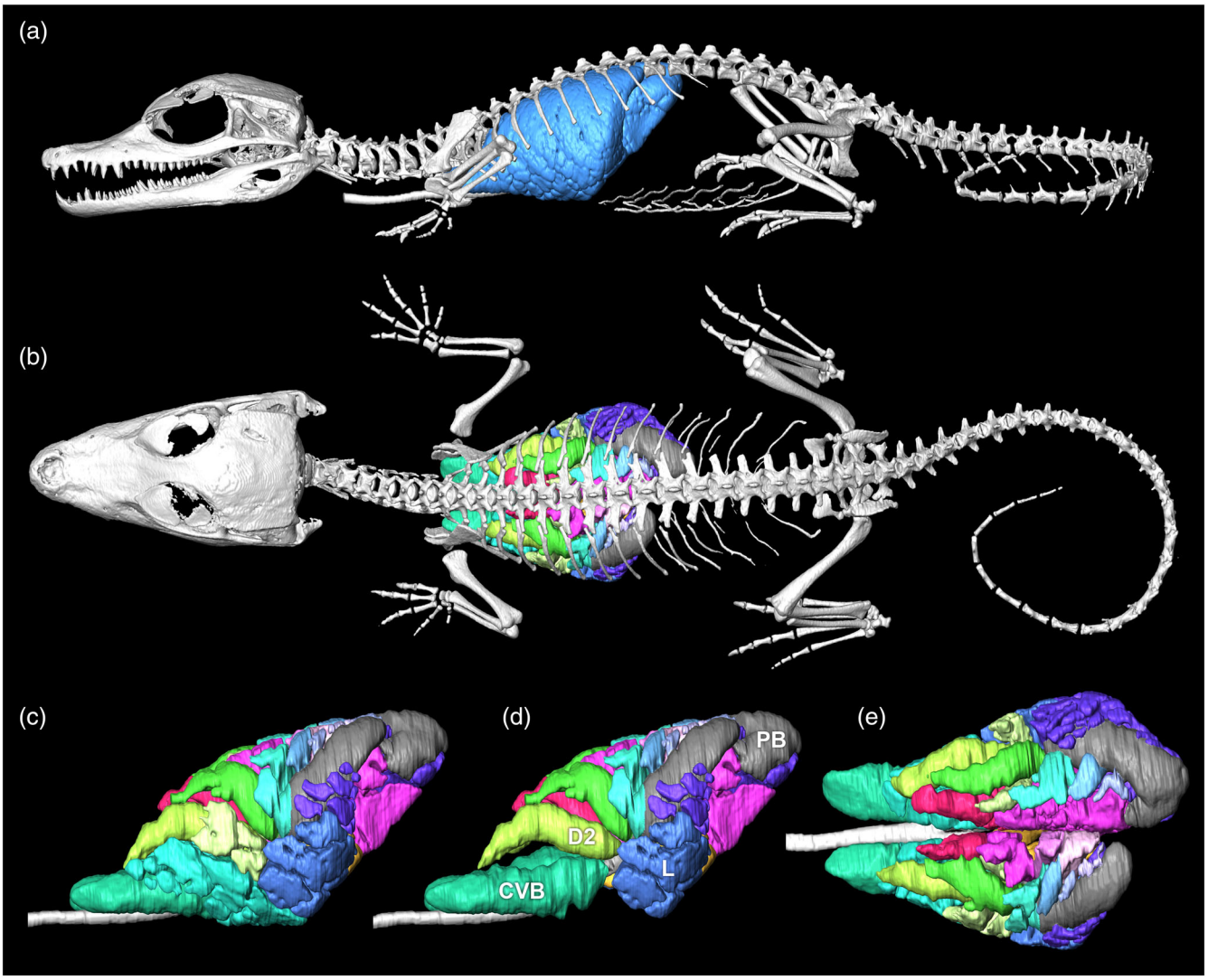

FIGURE 1 Skeletal and pulmonary anatomy of a deceased hatchling *Paleosuchus palpebrosus* (Sulla) during an artificial apnea. Segmented surface model of the skeleton and inflated lower respiratory system of *P. palpebrosus* in left lateral view (a) and dorsal view (b). Solid representation of the air spaces within the bronchial tree of Sulla in left lateral view with the tertiary bronchi present (c), removed (d), and rotated into dorsal view with all bronchi present (e). CVB, cervical ventral bronchi; D2, dorsal bronchus 2; L, laterobronchus; PB, primary bronchus

the fluid dynamic mechanisms maintaining these flow patterns in both avian and crocodilian clades remain poorly understood (Farmer, 2021). As a result, mapping bronchial architecture across the modern crocodilian phylogenetic tree (Oaks, 2011) is foundational for understanding the function and evolution of the respiratory system of this group. These data are particularly important for understanding how crocodilian lung morphology has changed since the origin of Archosauria, to test hypotheses regarding the functional constraints of unidirectional airflow, and to address adaptive questions associated with respiratory evolution in this group.

To date, the vast majority of anatomical work on crocodilians has been done on the American alligator (Allen et al., 2010; Crosby, 1917; Dodson, 1975; Hedrick et al., 2021; Holliday et al., 2013; Lessner & Holliday, 2020). Comparatively, the functional morphology of other crocodilian taxa has received considerably less attention with much of the research focusing instead on behavior, ecology, and systematics (Bittencourt et al., 2019; Campos et al., 2010; Campos et al., 2012). In terms of the respiratory morphology, to the best of our knowledge, only *A. mississippiensis* (Farmer & Sanders, 2010; Sanders & Farmer, 2012; Schachner et al., 2021) and *C. niloticus* (Perry, 1988; Schachner et al., 2013) have been reconstructed and described in detail in three dimensions making it difficult to understand which morphological characters relate to group wide trends within Crocodylia,

and which are specific to a given crocodilian taxon. With respect to the respiratory system of caimans, Gans and Clark (Gans & Clark, 1976) conducted a seminal and thorough investigation of the ventilatory mechanics of *C. crocodilus*. Their analysis included a description of the associated musculature (i.e., the abdominal, pelvic, intercostal muscles and diaphragmaticus muscle) but included no data on the internal pulmonary structures. Numerous caiman species have been used to investigate the physiology of gas exchange and ventilation mechanics in crocodilians (Malte et al., 2016; Reichert et al., 2019; Tattersall et al., 2006); however, pulmonary architecture has not been included.

Here we provide the first detailed three-dimensional (3D) description of caiman lung morphology and bronchial tree anatomy using Cuvier's dwarf caiman (*Paleosuchus palpebrosus*; Figure 1). Through a series of descriptive models of lung architecture and pulmonary measurements, we present the detailed gross anatomy of the lungs of three hatchlings and two adults. We additionally provide a comparison between *P. palpebrosus* and *A. mississippiensis* across a limited growth series (Schachner et al., 2021) which demonstrates which aspects of the bronchial tree are constrained as the lungs increase in size. Given the related respiratory biology of both *P. palpebrosus* and *A. mississippiensis*, we predict gross lung architecture and airway size and shape to be similar across both species due to functional constraints associated with unidirectional airflow patterns and the hepatic–piston ventilation system. These data provide a quantitative and qualitative framework for comparisons with other crocodilian species and a framework for evaluating homologous structures in crocodilian lungs.

2 | MATERIALS AND METHODS

2.1 | Terminology and homology

Terminology for the anatomy of the bronchial tree in *P. palpebrosus* follows that established by recent work for crocodilian lungs (Farmer, 2015b; Farmer & Sanders, 2010; Sanders & Farmer, 2012; Schachner et al., 2013, 2021). Hypotheses of homology in the bronchial tree between *P. palpebrosus* and *A. mississippiensis* are identified based upon anatomical similarities and shown with the same color scheme that matches that of Farmer and Sanders (2010) and Schachner et al. (2013, 2021). For ease of identifying individuals throughout the study, specimens are named for ancient Roman and Hellenistic kings and generals from the Late Republican period.

2.2 | Imaging and specimens

Computed tomographic (CT) and micro-computed CT (μCT) scans were collected from six specimens of Cuvier's dwarf caiman (*P. palpebrosus*; see Table 1 for the data on the specimens used in this study). Frozen/deceased hatchlings ($n = 3$) were obtained from private collections in southern Louisiana (death due to unknown causes). For this study: scans of one adult *P. palpebrosus* (Quintus Sertorius) were obtained by the San Antonio Zoo veterinary staff for unrelated clinical purposes and scans from a second adult (Mithridates) were obtained by MS Echols for clinical purposes from a privately owned facility, Scales and Tails Utah. This individual was scanned initially postprandially, and then again 9 months later in a fasted state. For the four deceased hatchlings, the specimens were intubated via either the glottis or directly through the trachea, and the lungs were inflated artificially by a polyethylene tube and syringe. One of the hatchlings, *P. palpebrosus* (Lucius Sulla), was imaged on a Nikon X-Tek HMXST 225 (Nikon Metrology Inc., Tokyo, Japan) μCT system at Harvard University's Center for Nanoscale Systems in Cambridge, MA. The second two hatchlings (Lucullus and Cinna) were dissected and scanned as torsos at the Louisiana State University School of Veterinary Medicine on a Scanco μCT 40 (SCANCO Medical AG, Brüttisellen, Switzerland). These two specimens were scanned at total lung capacity, and then scanned again open to atmosphere. This is to approximate functional residual capacity, and to visualize changes in the bronchial tree and lung position at the end of a hypothetical natural exhalation. The imaging data from the specimens are available via Data Dryad via the following links: (1) the alligators (https://datadryad.org/stash/dataset/doi:10.5061/dryad.3xsj3txdh); (2) the caimans (https://doi.org/10.5061/dryad.2bvq83bs0).

2.3 | Anatomical modeling, quantitative metrics, and analyses

3D surface models were segmented in Avizo 7.1 and 2020.3 (Thermo Fisher Scientific) following the methods established for extant archosaur lungs (Farmer & Sanders, 2010; Lawson et al., 2021; Sanders & Farmer, 2012; Schachner et al., 2013, 2017, 2021). For a detailed description of the segmentation methodology used, see Lawson et al. (2021). Bronchial tree colors in figures indicate proposed homologies and follow Schachner et al. (2021). Quantitative measurements of the airways were collected from the DICOM editor and viewer OsiriX MD (www.osirix-viewer.com) and are included in Table S1. These measures have been established in previous work (Lawson

TABLE 1 CT information and specimen data from the *Paleosuchus palpebrosus* included in this study

Specimen	Mass (kg)	Sex	Age	State of specimen	Scan resolution	Scanner	Scan location
Lucius Cornelius Sulla	0.06698	F	Hatchling	Deceased; intact	112 μm	Nikon X-Tek HMXST225	Harvard University
Lucullus	0.04252	?	Hatchling	Deceased; torso (inflated/open to atmosphere)	36 μm	Scanco μCT 40	LSU School of Veterinary Medicine
Cinna	0.04867	?	Hatchling	Deceased; torso (inflated/open to atmosphere)	36 μm	Scanco μCT 40	LSU School of Veterinary Medicine
Mithridates VI of Pontus	5	M	11	Live: (1) postprandial (entire animal), (2) fasting (torso)	(1) 200 μm (2) 250.2 μm	Epica GT-30 CT	Parrish Creek Veterinary Hospital and Diagnostic Center, Centerville, UT
Quintus Sertorius	12	M	40–45 years old (estimated; wild caught)	Live, torso	1.25 mm	GE Medical Systems LightSpeed QX/i	San Antonio Zoo

TABLE 2 *Alligator mississippiensis* specimens used from Schachner et al. (2021) for the quantitative comparisons in this study

Specimen	Mass (kg)	Age	State of specimen
Alligator AM041315-1	0.0757	Hatchling	Deceased; torso (inflated)
Alligator 15	1.7	Adult	Live, unsedated
Alligator 9	1.75	Adult	Live, unsedated
Alligator 739	2.8	Adult	Live, unsedated
Alligator 11	11	Adult	Live, unsedated

Note: Several alligators in Schachner et al. (2021) had imputed masses and only alligators with known masses were used in the present study.

et al., 2021; Schachner et al., 2021), and were based upon hypothesized homologous structures in other crocodilians (Farmer, 2015b; Sanders & Farmer, 2012; Schachner et al., 2013, 2021), as well as developmental work on reptiles and birds (Broman, 1939; Locy & Larsell, 1916a, 1916b). All measures were completed in the 3D MPR viewer of OsiriX. Additionally, each measure was completed by E. R. Schachner three times to eliminate interobserver error and averaged to reduce intraobserver error. Pulmonary metrics from the American alligators are derived from the specimens in Schachner et al. (2021) that have known body masses (Table 2).

To evaluate intraspecific variation and growth trends in *P. palpebrosus* and to make comparisons with that of *A. mississippiensis*, we collected the following metrics from the bronchial tree (Figure 2): (1) primary bronchus area at the origin of the cervical ventral bronchus (CVB), and first three dorsobronchi (D2–4); (2) the area of the ostium of the CVB and D2–4 at their origin from the primary bronchi; (3) the distance from the carina to the center of the CVB and D2–4. These metrics aim to capture lung shape and are homologous across both study taxa. Linear distances are reported in cm and areas in cm^2. Prior to analyses, all data were log10 transformed.

To assess differences in ontogenetic trajectories in lung measures, model II standard major axis (SMA) regressions were performed on the *P. palpebrosus* ($n = 4$) and *A. mississippiensis* ($n = 5$) metrics using the *lmodel2* v. 1.7-3 package in R (Legendre & Oksanen, 2018). When both axes are subject to error as in the case of body mass and pulmonary metrics, SMA regressions are preferred to ordinary least squares regressions (Sokal & Rohlf, 2012). Confidence intervals ($\alpha = .05$) were generated around slopes and intercepts for each regression using 999 permutations to assess deviations from isometry. However, given the small sample sizes for each taxon, these comparisons should be treated as preliminary. To visualize how the distance from the carina to each bronchus changed ontogenetically and differed

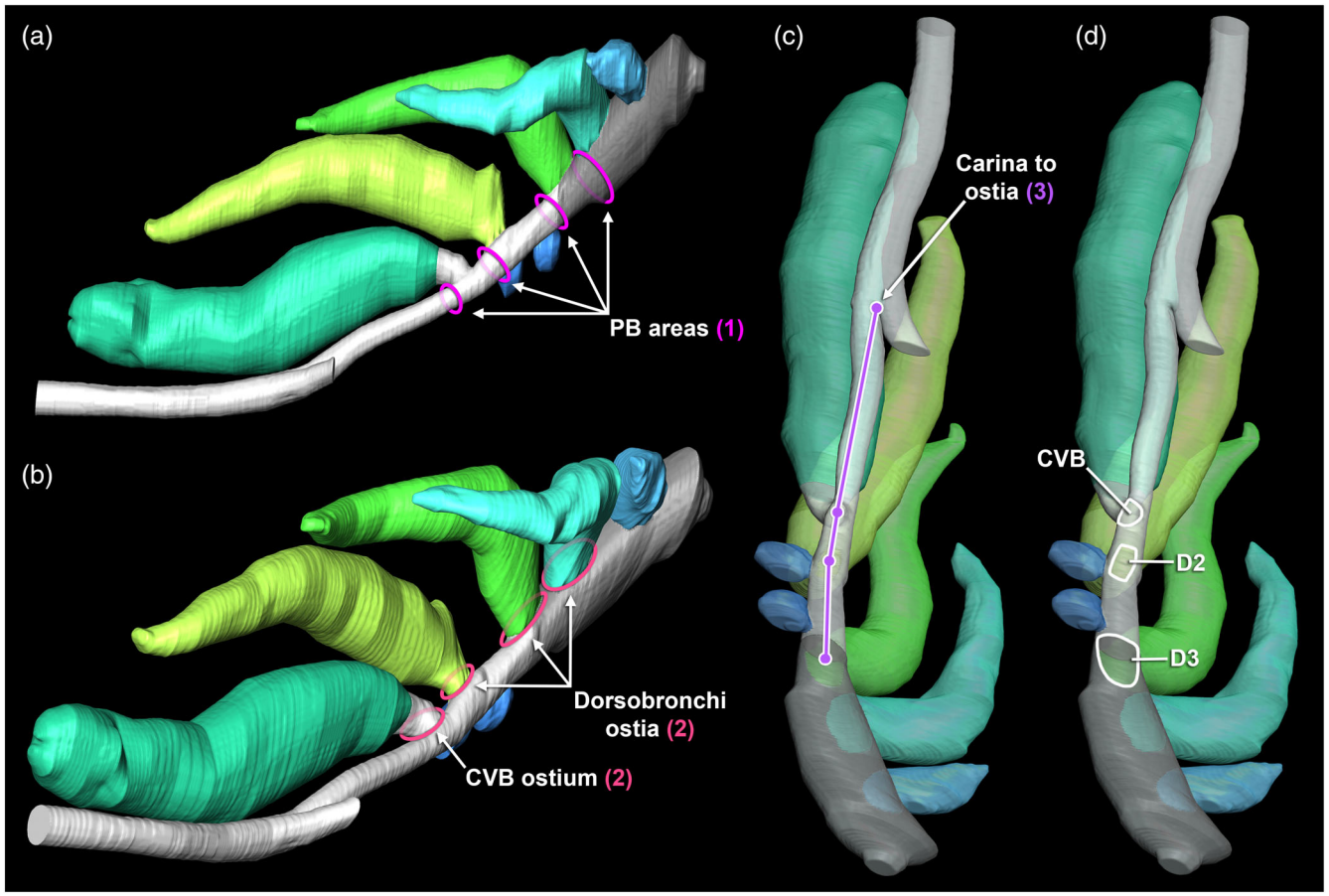

FIGURE 2 Diagrammatic model of *A. mississippiensis* showing the quantitative metrics. Reduced and simplified surface model of the right bronchial tree in medial (a), craniomedial (b), and ventral (c, d) views with the left lung, and medial, caudal, lateral, and tertiary bronchi all removed. These models are 3D digital representations of the locations of the 2D quantitative metrics collected from the DICOM imaging data (via OsiriX MD) following the methods of Schachner et al. (2021). Numbers represent locations of data collection: (1) area of the primary bronchus at the branching of the cervical ventral bronchus (CVB), and the origin of the first three dorsobronchi (D2–4); (2) the area of the ostium as it branches from the primary bronchus; (3) the distance from the carina to the center of the CVB and D2–3

between the two species, barplots showing percentages of distances from the carina to D3 were generated for both *A. mississippiensis* and *P. palpebrosus*.

3 | RESULTS

3.1 | Primary bronchus

In all individual caimans imaged, the primary bronchus is a proximally constricted tubular structure that balloons out distally toward the caudal aspect of the lung becoming saccular and giving off multiple secondary bronchi (the caudal group bronchi). The primary bronchus hooks around medially before attenuating into either a small point or a rounded blunt end (Figures 3a,c,e, 4 and 5). This medial hook-shaped curvature is similar to the morphology of alligators; however, the caimans possess fewer small sac-like structures projecting caudally off of the caudal aspect of the primary bronchus (Figure 6a–f).

3.2 | Cervical ventral bronchus

The cervical ventral bronchus (CVB) is a large tubular bronchus that branches off the primary bronchus from a cartilaginous cone-shaped ostium (Figures 3c,d and 5a,c). It is anatomically similar to its homologous structure in *A. mississippiensis* in all of the individuals imaged for this study. As in alligators, this bronchus makes a hairpin turn directly cranially toward the apex of the lung, after branching from the primary bronchus (Figure 5a–d). In all specimens, small tertiary branches emerged from the surface of the CVB along the proximal two-thirds of its length. In two caimans, Sertorius and Lucullus, large paired tubular tertiary bronchi branch from the dorsomedial aspect of the cartilaginous cone (Figure 5c) and

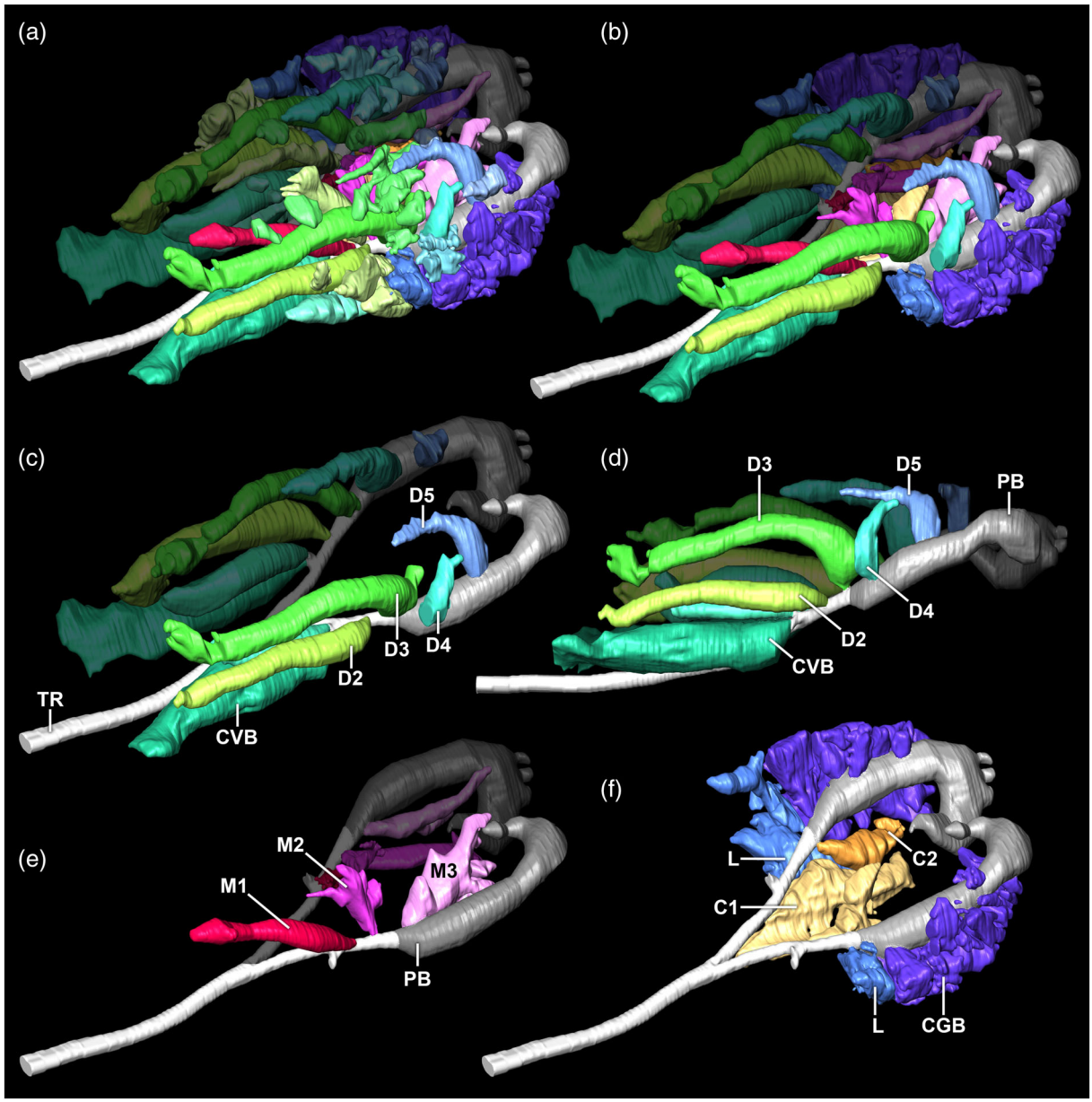

FIGURE 3 Anatomy of the bronchial tree. Digital segmented surface model of the bronchial tree (air spaces) in an adult live *P. palpebrosus* (Quintus Sertorius) during a natural apnea, with all images in left craniolateral view (except for D). The bronchial tree with the secondary and tertiary bronchi present (a), and then the same model with the tertiary bronchi removed (b). (c, d) The trachea, primary bronchi, cervical ventral bronchi, and dorsobronchi in isolation. (e) The primary airways and medial bronchi in isolation. (f) The primary airways with the cardiac branches and caudal group bronchi in isolation. The color scheme follows Schachner et al. (2021). C1–2, cardiac branches 1–2; CVB, cervical ventral bronchus; D1–5, dorsobronchi 1–5; L, laterobronchus; M1–3, medial bronchi 1–3; PB, primary bronchus; TR, trachea

extend cranially for at least half of the length of the CVB. This morphology was also observed in one of the alligators by Schachner et al. (2021).

3.3 | Dorsobronchi

In *P. palpebrosus*, the dorsobronchi (D) are large medially curving and craniodorsally projecting tapered tubular conduits that branch off of the intrapulmonary primary bronchus in a sequential manner, caudal to the cartilaginous cone of the CVB. This morphological arrangement is similar to alligators, with large D2–4 branches emerging off of the dorsal aspect of the primary bronchus (Figure 3c,d). However, the caimans measured for this study do not demonstrate a distinct D5 (the fourth dorsobronchus) as consistently as their alligator counterparts (Figure 5). Two individuals, Mithridates and Lucullus,

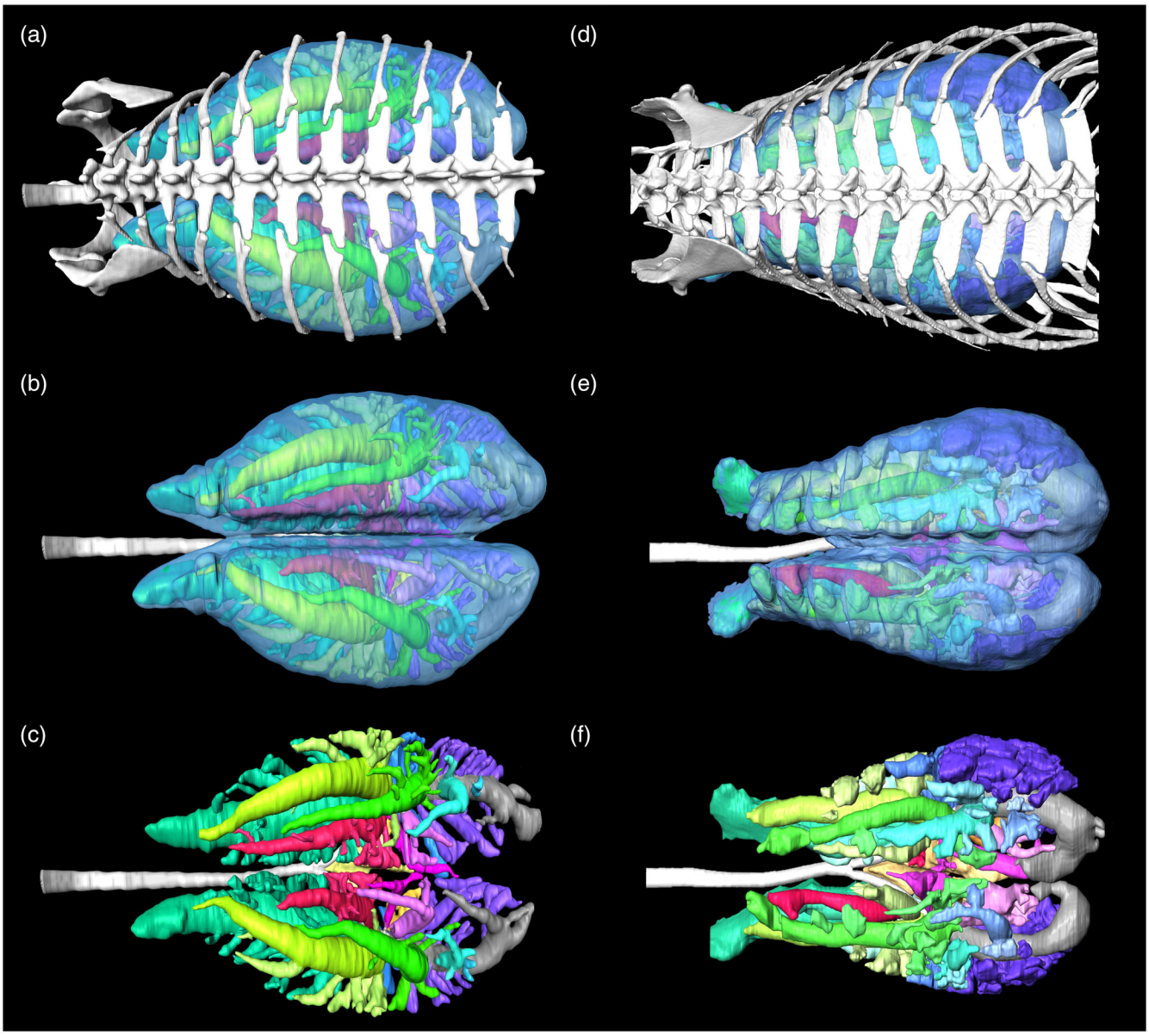

FIGURE 4 American alligator thorax versus a Cuvier's dwarf caiman thorax. Segmented model of the thorax and pectoral girdle (a), lung surface (b), and bronchial tree (c) of an 11 kg live American alligator (A. *mississippiensis*) and thorax and pectoral girdle (d), lung surface (e), and bronchial tree (f) of a 12 kg live Cuvier's dwarf caiman (*P. palpebrosus*). All images are in dorsal view. Images not to scale

have an accessory tubular bronchus that branches off the dorsolateral surface of the primary bronchus lateral to the dorsobronchial series, and while this may be an accessory or duplicated dorsobronchus, the identity of this bronchus cannot be confidently assigned.

3.4 | Medial bronchi

The medial bronchi (M) are substantially more variable than either the CVB or the dorsobronchi and show considerable bilateral asymmetry. The generally consistent pattern in the caimans is for a large medial bronchus (M1; Figure 3e) to branch from the primary bronchus immediately caudal to the CVB and travel cranially toward the apex of the lung. M1 is positioned dorsomedial to the CVB and ventromedial to D1 in most individuals. Some variation in this pattern is present. M1 in the right lung of Sertorius is extremely small and saccular in its overall shape. The position within the right lung that is usually occupied by M1 is occupied by a tertiary bronchus branching from D2 in this individual. This morphology is also the case in the hatchling Lucullus but mirrored with the tertiary dorsobronchus arising from D2 in the left lung. In the hatchling Cinna, M1 branches off caudal to D2 (Figure 5a) which is unusual in comparison

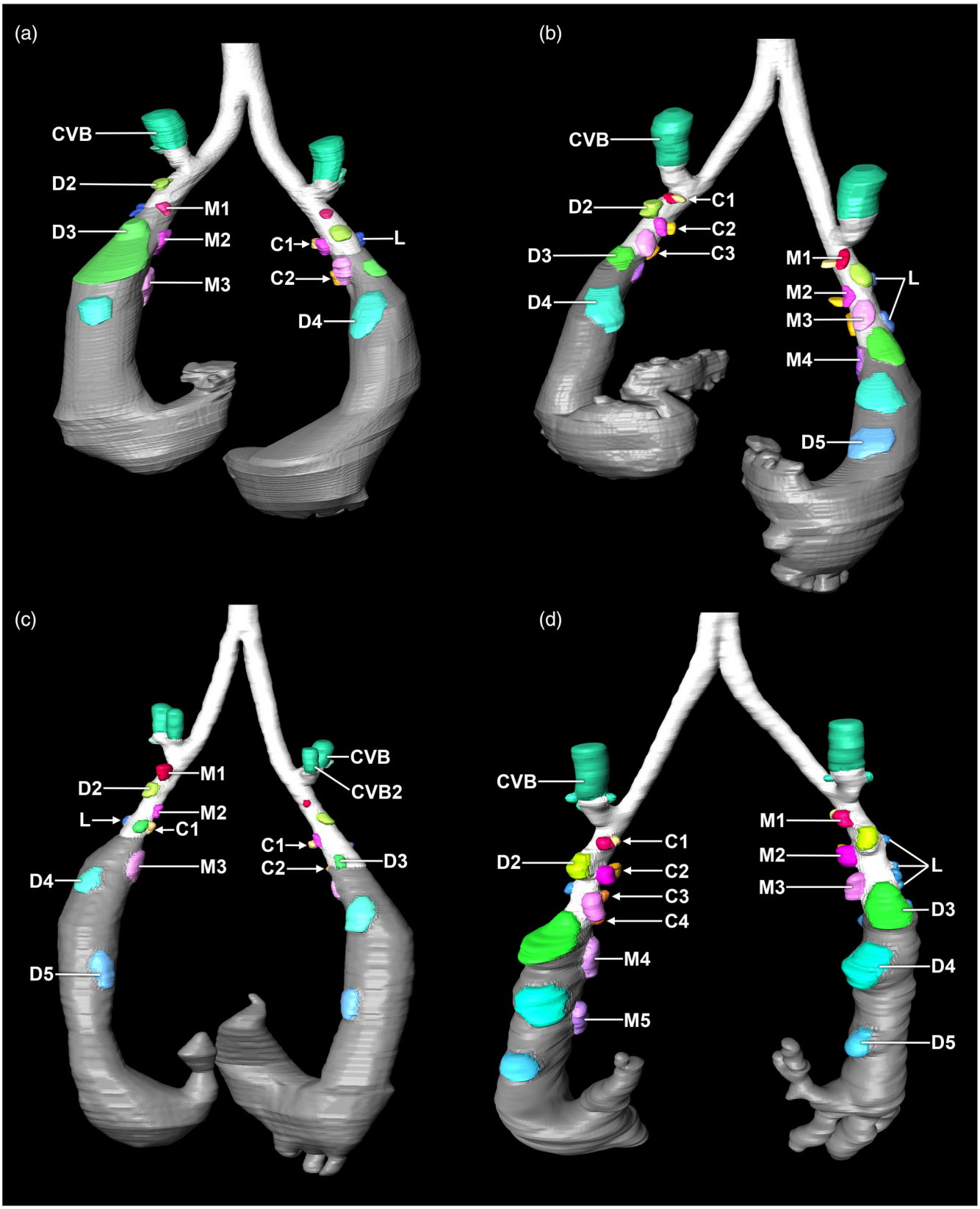

FIGURE 5 Segmented 3D surface model of the bronchial trees of hatchling and adult *P. palpebrosus* and *A. mississippiensis*. Surface models demonstrating the position and generalized size of the ostia of the major secondary airways of the *P. palpebrosus* hatchling Cinna (a) and adult Sertorius (c) and *A. mississippiensis* hatchling AM041315-1 (b) and adult 64 (d) in dorsal view. Images not to scale. C1–4, cardiac branches 1–4; CVB, cervical ventral bronchus; D1–5, dorsobronchi 1–5; L, laterobronchus; M1–4, medial bronchi 1–4; PB, primary bronchus. Colors represent hypotheses of homology and follow Schachner et al. (2021). Images not to scale

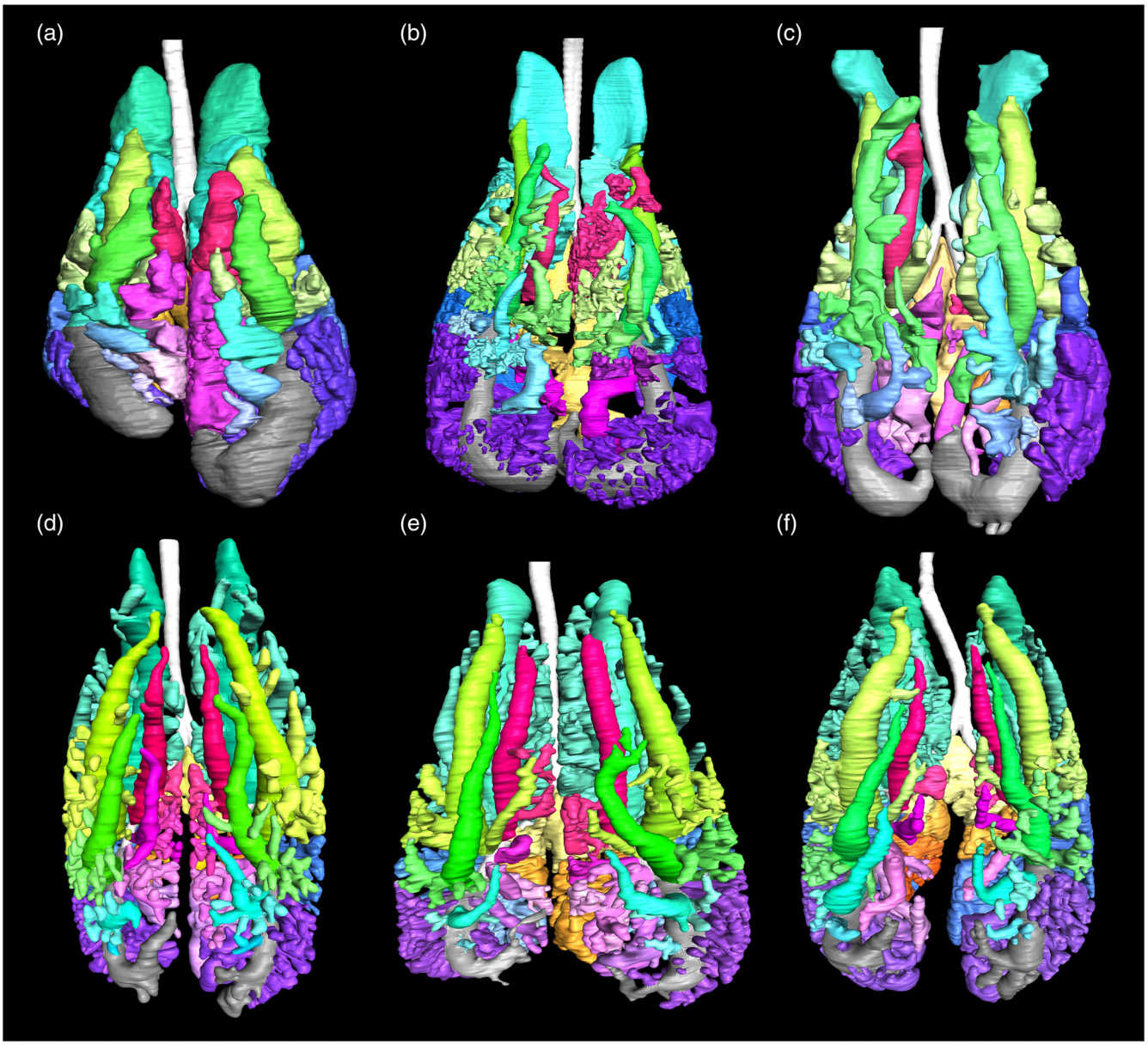

FIGURE 6 Intra- and interspecific variation in the bronchial tree. Segmented surface models of the bronchial tree for three different *P. palpebrosus* (a–c) and three different A. *mississippiensis* (d–f) specimens in dorsal view. All of the individual specimens were scanned live during a natural or sedated apnea with the exception of (a), the deceased hatchling (Sulla). (b) Mithridates (*P. palpebrosus*, 5 kg); (c) Sertorius (*P. palpebrosus*, 12 kg); (d) alligator 15 (*A. mississippiensis*, 1.7 kg); (e) stumpy (*A. mississippiensis*, 13.4 kg); (f) alligator 64 (*A. mississippiensis*, 14.5 kg). Images not to scale

to the other caimans and alligators we have imaged. The more caudally positioned medial branches are even more variable in *P. palpebrosus* ballooning into large saccular structures in some (Sulla; Figures 1a and 6a) and remaining more tubular in others (Mithridates and Sertorius; Figure 6b,c). Notably, the caimans overall tend to have fewer medial bronchi than the alligators, which were recorded to have up to five branches on one side (Schachner et al., 2021).

3.5 | Laterobronchi

The laterobronchi (L) are proximally constricted, distally voluminous sac-shaped bronchi that emerge off of the lateral and ventral surfaces of the primary bronchus (Figure 3f). These airways branch around the location of D2 or just caudal to the first dorsobronchus. Similar to the bronchial anatomy observed in alligators, the laterobronchi in *P. palpebrosus* demonstrate bilateral asymmetry in some

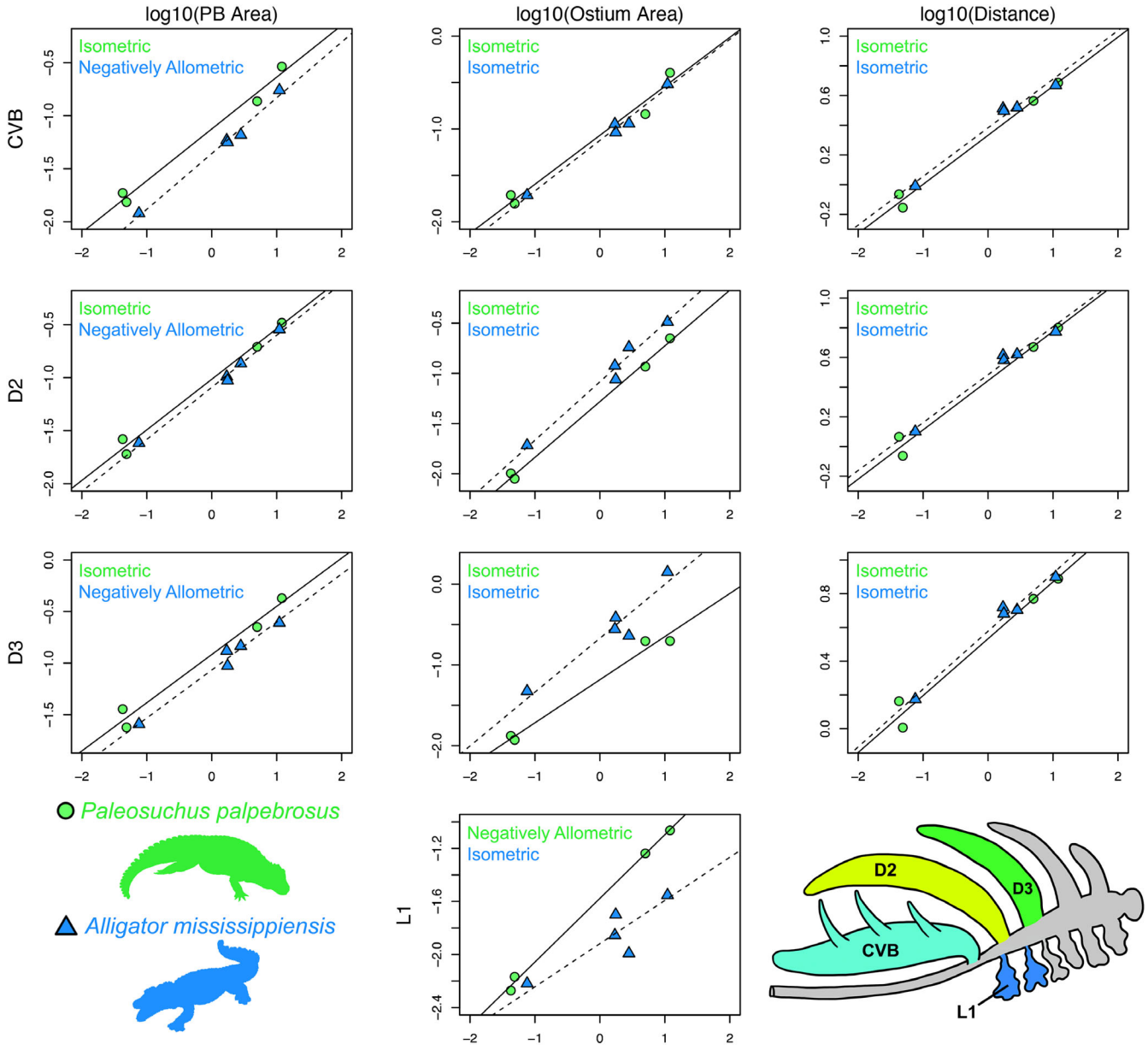

FIGURE 7 Standard major axis regressions for 10 lung metrics against log10-transformed body mass. The *x*-axis represents log10-transformed body mass in all plots. The first column represents log10-transformed PB area against body mass. The second column represents log10-transformed ostium area against body mass, and the third column represents log10-transformed distance to the carina against body mass. Rows represent the CVB (top row), then D2, D3, and L1 (for which only ostium area was measured). *P. palpebrosus* is represented as green circles and *A. mississippiensis* is represented by blue triangles. The solid line represents the SMA regression for *P. palpebrosus*. The dashed line represents the SMA regression for *A. mississippiensis*

instances (e.g., one on the left lung and two on the right in the hatchling Cinna) and symmetry in others (ranging from one laterobronchus in each lung in Sertorius to three on each primary bronchus in Mithridates).

3.6 | Caudal group bronchi

As in *A. mississippiensis*, there are numerous saccular bronchi that emerge from the caudoventral region of the primary bronchus in *P. palpebrosus*. There are variably small additional caudal group bronchi (CGB) in some individuals (e.g., Mithridates) that branch off of the lateral, medial, and dorsal surfaces as well (Figure 6b). The morphology of these airways is grossly similar to the laterobronchi in that they are grossly blind saccular structures; however, the overall shape diverges in that they are effectively hexagonal air sacs with wide ostia. It is unknown if there are small inter-bronchial perforations between the individual CGB, but none were visible

TABLE 3 *Alligator mississippiensis* ($n = 5$) standard major axis regression results showing slopes and y-intercepts with 95% confidence intervals, the value for isometry for each measure, and the trend

	Lower CI	Slope	Upper CI	Lower CI	y-intercept	Upper CI	Isometry	Trend
CVBPBArea	0.436	0.525	0.633	−1.375	−1.357	−1.342	0.66	Neg
CVBOstArea	0.438	0.544	0.676	−1.145	−1.123	−1.105	0.66	Iso
CVBDist	0.241	0.327	0.445	0.363	0.383	0.397	0.33	Iso
D2PBArea	0.415	0.490	0.580	−1.107	−1.092	−1.079	0.66	Neg
D2OstArea	0.436	0.583	0.779	−1.117	−1.084	−1.059	0.66	Iso
D2Dist	0.243	0.322	0.428	0.466	0.484	0.497	0.33	Iso
D3PBArea	0.353	0.465	0.614	−1.092	−1.067	−1.048	0.66	Neg
D3OstArea	0.391	0.667	1.138	−0.749	−0.670	−0.623	0.66	Iso
D3Dist	0.261	0.343	0.450	0.560	0.578	0.592	0.33	Iso
D4PBArea	0.142	0.326	0.745	−1.989	−1.918	−1.887	0.66	Iso

Note: Iso, isometry; Neg, negative allometry; Pos, positive allometry.
Abbreviations: CVB, cervical ventral bronchus; D2, dorsobronchus 2; D3, dorsobronchus 3; D4, dorsobronchus 4; PBArea, area of primary bronchus at each origin of ostium; OstArea, area of ostium at each bronchus; Dist, distance from carina to each bronchus.

TABLE 4 *Paleosuchus palpebrosus* ($n = 4$) standard major Axis regression results showing slopes and y-intercepts with 95% confidence intervals, the value for isometry for each measure, and the trend

	Lower CI	Slope	Upper CI	Lower CI	y-intercept	Upper CI	Isometry	Trend
CVBPBArea	0.343	0.488	0.695	−1.158	−1.125	−1.078	0.66	Iso
CVBOstArea	0.325	0.528	0.858	−1.114	−1.068	−0.993	0.66	Iso
CVBDist	0.242	0.331	0.452	0.312	0.333	0.360	0.33	Iso
D2PBArea	0.337	0.477	0.674	−1.047	−1.015	−0.971	0.66	Iso
D2OstArea	0.458	0.555	0.673	−1.304	−1.282	−1.255	0.66	Iso
D2Dist	0.219	0.332	0.502	0.418	0.444	0.483	0.33	Iso
D3PBArea	0.297	0.467	0.736	−0.955	−0.917	−0.856	0.66	Iso
D3OstArea	0.365	0.534	0.782	−1.222	−1.183	−1.127	0.66	Iso
D3Dist	0.208	0.337	0.546	0.504	0.534	0.581	0.33	Iso
D4PBArea	0.413	0.480	0.558	−1.592	−1.577	−1.559	0.66	Neg

Note: Iso, isometry; Neg, negative allometry; Pos, positive allometry.
Abbreviations: CVB, cervical ventral bronchus; D2, dorsobronchus 2; D3, dorsobronchus 3; D4, dorsobronchus 4; PBArea, area of primary bronchus at each origin of ostium; OstArea, area of ostium at each bronchus; Dist, distance from carina to each bronchus.

TABLE 5 Means and standard deviations for distances from the carina to the CVB and each of the major measurable secondary dorsobronchi for *A. mississippiensis* and *P. palpebrosus*

Species	Bronchus (distance)	Mean	Standard deviation
A. mississippiensis	CVB	63.41	2.86
A. mississippiensis	D2	16.54	1.68
A. mississippiensis	D3	20.05	3.69
P. palpebrosus	CVB	63.26	4.09
P. palpebrosus	D2	18.37	1.91
P. palpebrosus	D3	18.37	2.61

via CT or μCT. There is considerable variation in CGB morphology with no obvious pattern between bronchus size and specimen age. The hatchling Sulla (Figure 6a) and the adult Sertorius (Figure 6c) have large voluminous CGB, while the slightly smaller adult Mithridates (Figure 6b) has a multitude of small CGB.

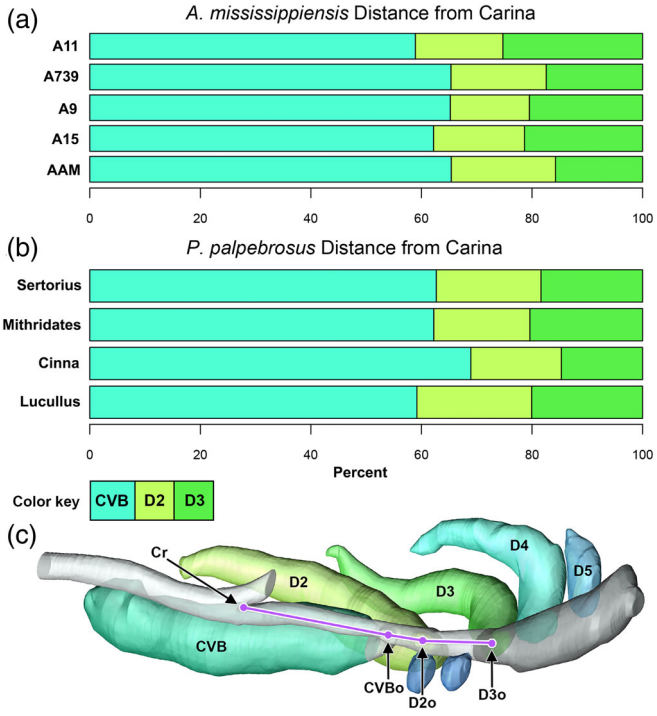

FIGURE 8 Ratio of the distances from the carina to the major secondary branches in alligators and dwarf caimans. Distances from the carina to each bronchus represented as a percentage of total length (from the carina to D3) for (a) *A. mississippiensis* and (b) *P. palpebrosus*. (c) Simplified model of the right bronchial tree of a hatchling alligator (in ventral view) demonstrating the metrics collected in both taxa. CVB, cervical ventral bronchus; CVBo, cervical ventral bronchus ostium; Cr, carina; D2–D5, dorsobronchi 2–5; D2o, dorsobronchus 2 ostium; D3o, dorsobronchus 3 ostium

3.7 | Cardiac bronchi

The anatomy of the cardiac bronchi is considerably asymmetric (Figure 3f), with one large bronchus occupying the space between the left and right primary bronchi and reaching the carina predominantly from one lung in all individuals. In Sertorius, two branches contribute to the cardiac bronchi or "lobes," with the primary and cranial-most cardiac bronchus (C1) arising from the right primary bronchus (Figure 5c). The smaller corresponding cardiac bronchus on the left side typically emerge from the second medial bronchus. In the hatchling Cinna, branches contributing to the cardiac region only emerge from the right lung (Figure 5a). In Sulla, the larger and more cranially positioned cardiac bronchus emerges from the right, with a smaller slightly caudally positioned cardiac bronchus arising on the left lung. Mithridates has a similar morphology to Sulla, with the larger cranially positioned cardiac bronchus emerging from the right lung, and the smaller cardiac bronchus branching from the left lung. In comparison to the alligator, there was an overall reduced number of bronchi contributing to the cardiac lobes. Schachner et al. (2021) observed that alligators can have up to four bronchi contributing, with a general pattern of 3/3 on each side. Every alligator imaged had larger and more cranial cardiac lobes emerging the right lung, and we found this to also be the case in *P. palpebrosus*.

3.8 | Pulmonary measures

All confidence intervals for the lung measurements overlap between *A. mississippiensis* and *P. palpebrosus*, so there are no differences between the taxa in their ontogenetic trajectories for these metrics (Figure 7; Tables 3–5). However, it is important to note that low sample sizes led to the generation of large confidence intervals, and it is best to view these data as preliminary. Considering that most of the *P. palpebrosus* did not have a D5, and when the D4 was present, the ostium was often too ambiguous to measure, only the CVB, D2, D3, and L1 (only ostium area) are directly comparable between the two taxa (Figures 7 and 8). The distance from the carina to the ostium of the CVB, D2, and D3 in the caimans is consistent across the four individuals measured and grows isometrically, similar to that found in alligators (Figure 7). Ostium area similarly grows isometrically for the CVB, D2, and D3 for both taxa (Figure 7). The primary bronchus area at the CVB, D2, and D3 grows isometrically in *P. palpebrosus* whereas they grow with negative allometry in *Alligator*. To assess the positioning of bronchi relative to the carina, the distances from the carina to the CVB, D2, and D3 were converted to percentages of total length in each specimen and then a mean and standard deviation were taken. The average distances from the carina to the CVB were nearly the same for *A. mississippiensis* (Mean = 63.41%, *SD* = 2.86) and *P. palpebrosus* (mean = 63.26%, *SD* = 4.09). The distances from the CVB to D2 and D2 to D3 were quite similar as well across the two species (Figure 8).

4 | DISCUSSION

4.1 | *Paleosuchus* versus *Alligator*

Our data demonstrate that there are clear and consistent patterns in pulmonary morphology shared by *A. mississippiensis* and *P. palpebrosus*. These are (a) the primary bronchus begins as a narrowly constricted tube and expands caudally, bending medially into a hook-shaped structure; (b) the CVB branches off first after making a hairpin turn, is a long tube-shaped bronchus,

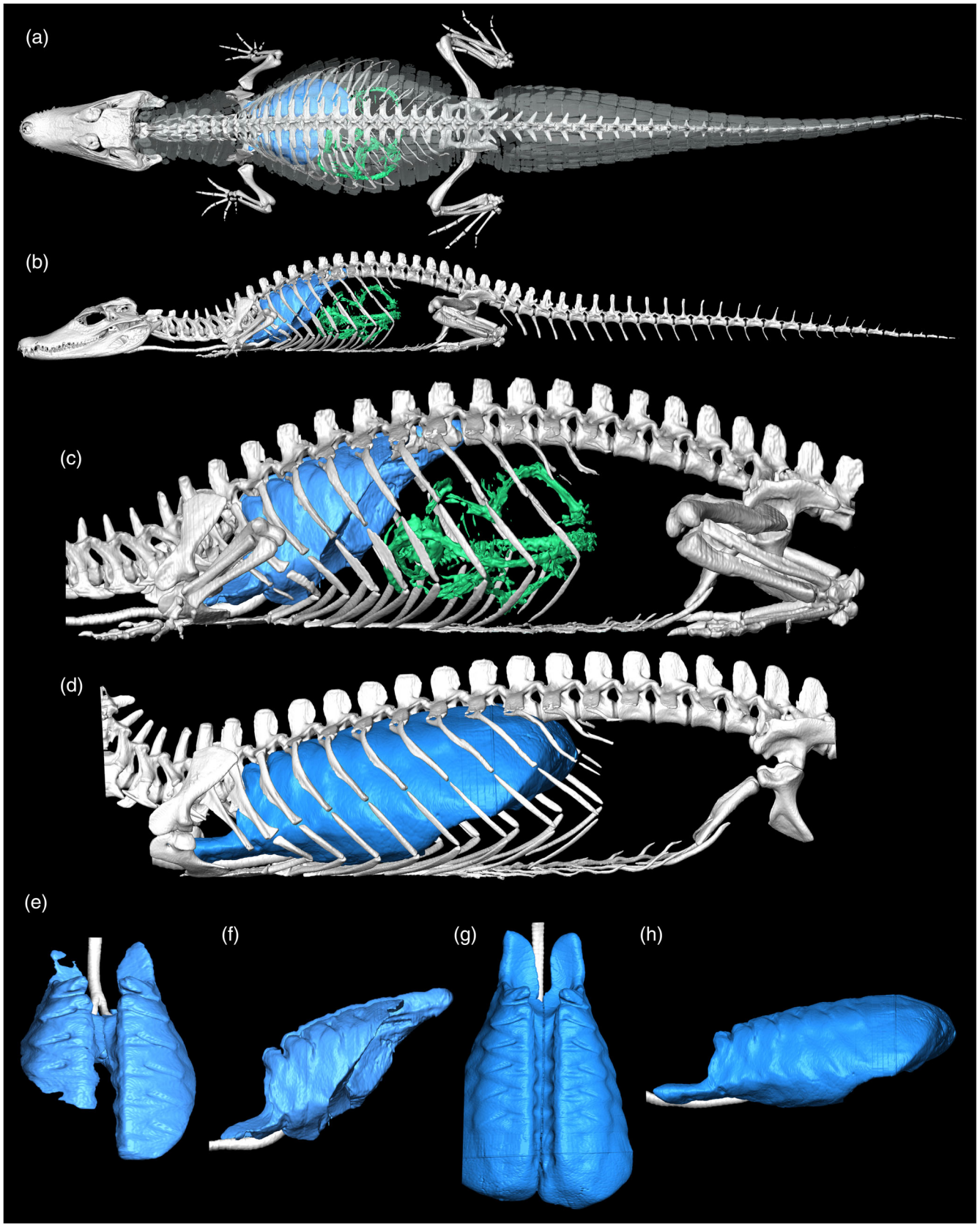

FIGURE 9 Fasting and postprandial morphology of *P. palpebrosus* (Mithridates, 5 kg). Skeletal model and lung surface model of a live *P. palpebrosus* in dorsal (a, with the scutes visible) and in left lateral views (b, c), approximately 2–3 hours after ingesting a large rat. The partially digested rat skeleton is identified in green. (d) Thorax model of the same animal after a fast in left lateral view. The isolated lungs from the postprandial model are shown in dorsal (e) and left lateral (f) views. The isolated lungs from the fasting model are shown in dorsal (g) and left lateral (h) views. Images not to scale

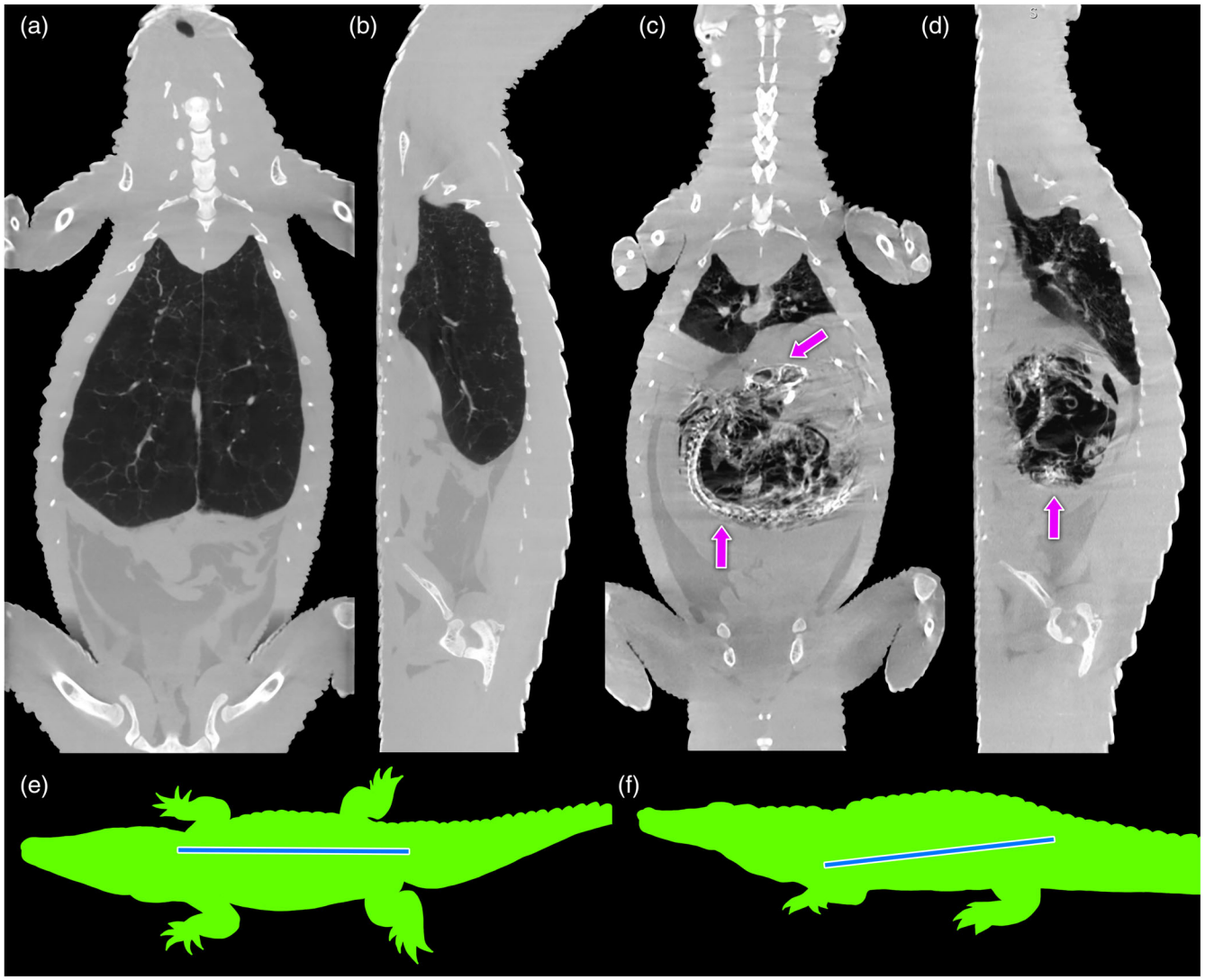

FIGURE 10 Coronal and sagittal CT images of the lungs of an adult *Paleosuchus* in a fasted and postprandial state. CT images of the lungs and torso of Mithridates in a fasted state shown in coronal (a) and sagittal (b) views, and after having eaten a large rat in coronal (c) and sagittal views (d,e) Diagrammatic demonstration of where the sagittal image slices were taken in (b and d), and where the coronal image slices were taken in (a) and (c). Pink arrows indicate the undigested rat skeleton

and reaches the apex of the lung; (c) a series of dorsobronchi branch off of the primary bronchus sequentially in a row; (d) a series of highly variable medial bronchi branch off of the primary bronchus; (e) a series of proximally constricted and distally ballooned laterobronchi branch off of the ventrolateral surface of the primary bronchus; and (f) a series of grossly dead end tubular sac-like CGBs arise from the caudal region of the primary bronchus (Figure 6). Additionally, there are no statistical differences in ontogenetic allometry for lung metrics (Figure 7), and the relative distances from the carina to the CVB, D2, and D3 are nearly identical across both taxa (Figure 8).

The substantive differences between the two taxa are in the bronchial numbers and in the caudal regions of the lungs. Alligators show increased bronchial contributions to the cardiac "lobes"—up to four bronchi in some individuals (Schachner et al., 2021), and a more consistent presence of a fourth dorsobronchus (D5). Additionally, the area of the primary bronchus scales with negative allometry at the CVB, D2, and D3 in *A. mississippiensis* while it scales with isometry in these regions in *P. palpebrosus* (Tables 3 and4). Despite these differences, the large number of similarities between taxa suggest that unidirectional airflow may be constraining lung morphology in crocodilians. This is particularly true in the more proximal regions of the bronchial tree, around the CVB and first few dorsobronchi. Segmented models of juvenile Nile crocodile (*C. niloticus*) lungs show a similar overall morphology as the two species analyzed

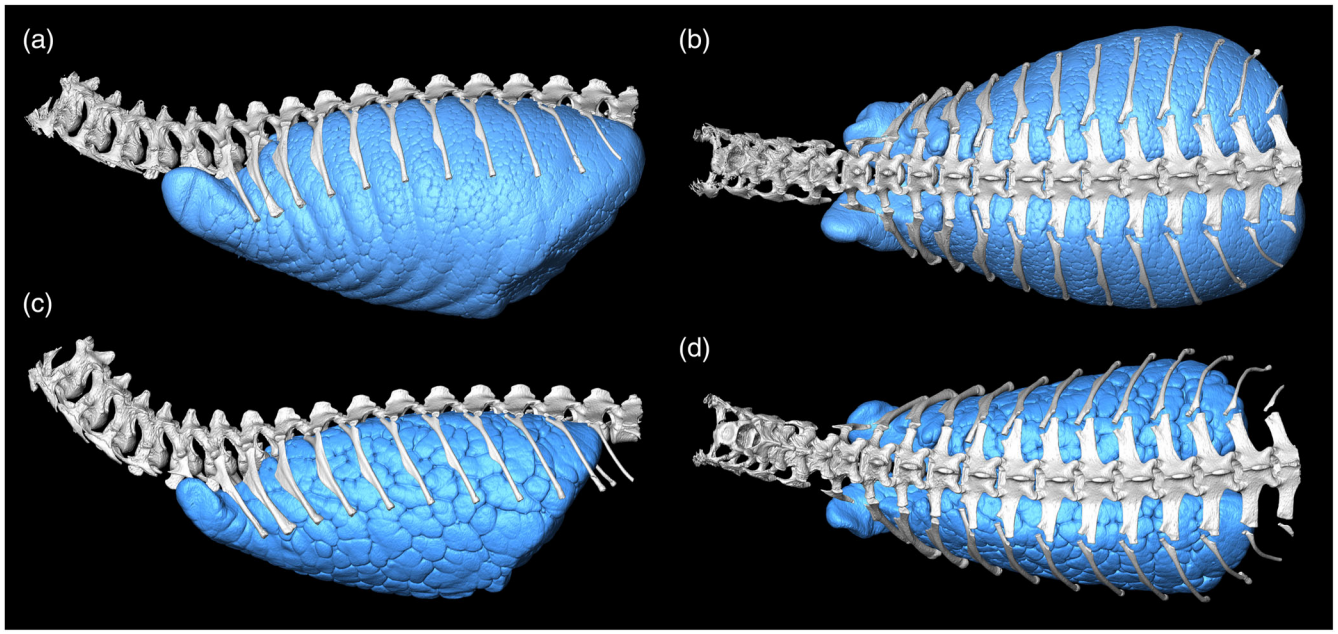

FIGURE 11 Total lung capacity versus open to atmosphere. Surface model of the lungs and partial axial skeleton (vertebrae and dorsal ribs) in left lateral (a,b) and dorsal (c,d) views of a deceased hatchling *P. palpebrosus* (Lucullus). The torso was fully inflated under positive pressure (a,c), and left open to atmosphere (b,d) demonstrating the different position of the lungs relative to the vertebral column at total lung capacity versus when air leaves the lungs due to gravity and the pressure of the surrounding tissues

for this study, but an increased number of secondary bronchi in the caudal half of the lung (Schachner et al., 2013). It is unclear whether these differences are phylogenetic, environmental, or due to another unknown factor. Additional taxa must be evaluated (e.g., more basal crocodilians like *Tomistoma schlegelii*, *Gavialis gangeticus*, and other non-alligatoroid species) to determine if these traits are ubiquitous across all crocodilians and to what extent the results can be used to reconstruct the ancestral crocodilian lung.

4.2 | Shifts in pulmonary position

Position of the lungs and associated viscera within the thoracocoelomic cavity of crocodiles has been a topic of interest for biologists and paleontologists for a variety of reasons related to investigating the evolution of ventilation in archosaurs (Brocklehurst et al., 2018, 2020; Radermacher et al., 2021; Schachner et al., 2009, 2011). Uriona and Farmer (2008) demonstrated through electromyography that *A. mississippiensis* can actively recruit select abdominal and pelvic muscles, along with the novel m. diaphragmaticus muscle (which encapsulates the abdominal viscera) to shift the organs during aquatic locomotion. Whether or not the lungs themselves are translating relative to the thoracic ceiling during ventilation and how this impacts the bronchial tree is still unknown. Schachner et al. (2009, 2011) and Brocklehurst et al. (2018, 2020) associated the flat thoracic ceiling of extant crocodilians with this "hepatic-piston" mechanism and used it to reconstruct patterns of lung evolution in extinct taxa. Mithridates, a live 5 kg male individual, was imaged a few hours after eating a large rat (Figures 9a–c, e,f and 10) and then for a second time 9 months later while fasting and during a natural apnea (Figures 9d,g,h and 10). Immediately postprandially, the lung volume during the natural apnea decreased bilaterally due to the displacement by the rat carcass. Additionally, the lungs were shifted approximately five vertebral segments cranially on the left side and four on the right to accommodate the food bolus (Figures 9c,d and 10). Two of the hatchlings, Lucullus and Cinna, were imaged via μCT fully inflated and then scanned again open to atmosphere. In the fully inflated lungs of Lucullus, the caudal aspect of the left lung extends just under one and a half vertebral lengths longer than when the lungs were left open to atmosphere (Figure 11). This indicates that in deceased specimens, the visceral and parietal pleura are capable of sliding relative to one another craniocaudally. These data preliminarily validate previous attempts to use the smooth thoracic ceiling as an osteological correlate for pulmonary surface structure in extinct crocodilians (see, e.g., Brocklehurst et al., 2018, 2020; Schachner et al., 2009, 2011). However, the most important questions remain: (a) What are the pulmonary tissues doing

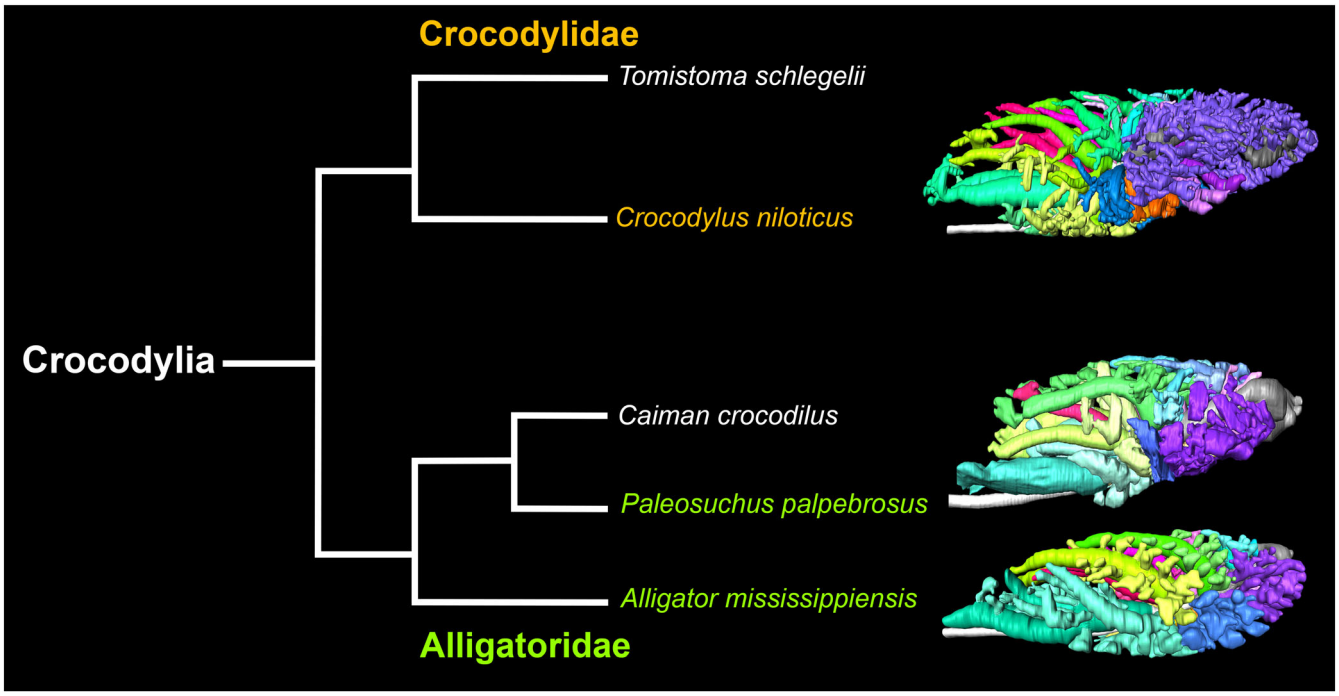

FIGURE 12 Phylogeny for Crocodylia and associated bronchial tree models. Simplified phylogeny for Crocodylia modified from Oaks (2011) showing the species represented in this study. Bronchial tree model for *Crocodylus niloticus* (NNC9) from Schachner et al. (2013). *Paleosuchus* model is Quintus Sertorius. *A. mississippiensis* model is "alligator 15" from Schachner et al. (2021). All models are in left lateral view, and not to scale

during active ventilation? (b) Are they translating relative to the thoracocoelomic body wall during different types of locomotion? Additional data on live crocodilian ventilation are needed to fully address these questions.

4.3 | Reconstructing the ancestral crocodilian lung

Reconstructions of pulmonary anatomy in extinct taxa have been of great interest over the last 20 years to paleontologists and biologists (Farmer, 2006; O'Connor, 2006, 2009; O'Connor & Claessens, 2005; Schachner et al., 2011; Sereno et al., 2008; Wedel, 2003, 2009). However, the details of crocodilian lung evolution have rarely been the focus of these analyses aside from discussions of the hepatic-piston ventilation mechanism and how it relates to dinosaurian ventilation or the ancestral archosaurian respiratory system (Brocklehurst et al., 2020; Radermacher et al., 2021; Scavezzoni & Fischer, 2021). More data on a variety of extant taxa are required to properly understand the origin and evolution of the crocodilian bronchial tree, including the origin of the hepatic–piston system.

Within extant crocodiles, basic questions remain regarding which aspects of the respiratory system are shared across the group and which components are unique to individual taxa. It has been demonstrated in numerous studies that every species of crocodilian examined exhibits unidirectional airflow patterns in various regions of the bronchial tree (Farmer, 2015b; Farmer & Sanders, 2010; Schachner et al., 2013). Each of these taxa has a large tubular bronchus that branches off the primary bronchus (the CVB), multiple secondary airways, a hook-shaped primary bronchus, and varying saccular airways (or air sacs) that extend into the lateral and caudal regions of the lung (Figure 12). What varies is the length of trachea and looping of the primary bronchus proximal to the carina (Farmer, 2015b), the number of secondary airways and the size of these branches, and the density of the respiratory parenchyma. While *Alligator* and *Paleosuchus* are superficially relatively similar, lungs of juvenile specimens of *C. niloticus* show an increased number of secondary bronchi relative to other crocodilians (Figure 12; Schachner et al., 2013) indicating that there could be ecological or phylogenetic differences impacting respiratory biology across the clade that necessitate further investigation. These data will prove useful for comparisons with avian taxa as more structural similarities and differences between crocodilians and birds emerge and are available for quantitative analyses. These results lay the groundwork to elucidate the basic bauplan

for alligatoroid lungs and generate hypotheses of homology for pulmonary structures across the entire crocodilian and archosaurian clades.

ACKNOWLEDGMENTS

This research was supported by LSUHSC Research Enhancement Program New Project Grants to Emma R. Schachner and Brandon P. Hedrick. Special thank you to Scales and Tails Utah for permission to use scans of their animals, and two anonymous reviewers who improved the manuscript considerably. Some of the μCT image data (Lucullus and Cinna) were produced by the Louisiana State University School of Veterinary Medicine's μCT. This work was performed in part at the Harvard University Center for Nanoscale Systems (CNS), a member of the National Nanotechnology Coordinated Infrastructure Network (NNCI), which is supported by the National Science Foundation under NSF ECCS award no. 1541959. The authors declare no conflict of interest.

AUTHOR CONTRIBUTIONS

Emma R. Schachner: Conceptualization (lead); data curation (lead); formal analysis (lead); funding acquisition (lead); investigation (lead); methodology (lead); project administration (lead); resources (lead); software (lead); visualization (lead); writing – original draft (lead); writing – review and editing (lead). **Raul Eduardo Diaz:** Conceptualization (supporting); data curation (supporting); resources (supporting); writing – review and editing (equal). **Rob Coke:** Data curation (supporting); funding acquisition (supporting); investigation (supporting); methodology (supporting); resources (supporting); writing – review and editing (equal). **M. Scott Echols:** Data curation (supporting); methodology (supporting); resources (supporting); writing – review and editing (equal). **Michelle L. Osborn:** Data curation (supporting); methodology (supporting); resources (supporting); writing – review and editing (equal). **Brandon Hedrick:** Conceptualization (equal); data curation (equal); formal analysis (equal); funding acquisition (equal); methodology (equal); software (equal); writing – review and editing (equal).

ORCID

Emma R. Schachner https://orcid.org/0000-0002-8636-925X
Raul E. Diaz https://orcid.org/0000-0001-9107-124X
Michelle L. Osborn https://orcid.org/0000-0003-0811-9279
Brandon P. Hedrick https://orcid.org/0000-0003-4446-3405

REFERENCES

Allen, V., Elsey, R. M., Jones, N., Wright, J., & Hutchinson, J. R. (2010). Functional specialization and ontogenetic scaling of limb anatomy in *Alligator mississippiensis*. *Journal of Anatomy*, *216*, 423–445.

Bittencourt, P. S., Campos, Z., de Lima, M. F., Marioni, B., Souza, B. C., Da Silveira, R., de Thoisy, B., Hrbek, T., & Farias, I. P. (2019). Evidence of cryptic lineages within a small south American crocodilian: The Schneider's dwarf caiman *Paleosuchus trigonatus* (Alligatoridae: Caimaninae). *PeerJ*, *7*, e6580.

Brocklehurst, R. J., Schachner, E. R., Codd, J. R., & Sellers, W. I. (2020). Respiratory evolution in archosaurs. *Philosophical Transactions of the Royal Society B*, *375*, 20190140.

Brocklehurst, R. J., Schachner, E. R., & Sellers, W. I. (2018). Vertebral morphometrics in non-avian dinosaurs. *Royal Society Open Science*, *5*, 180983.

Broman, I. (1939). Die embryonalentwicklung der lungen bei krokodilen und seesschildkröten. *Jahrbuch für Morphologie Mikroskopisch-Anatomische*, *84*, 224–306.

Campos, Z., Sanaiotti, T., & Magnusson, W. E. (2010). Maximum size of dwarf caiman, *Paleosuchus palpebrosus* (Cuvier, 1807), in the Amazon and habitats surrounding the Pantanal, Brazil. *Amphibia-Reptilia*, *31*, 439–442.

Campos, Z., Sanaiotti, T., Muniz, F., Farias, I., & Magnusson, W. E. (2012). Parental care in the dwarf caiman, *Paleosuchus palpebrosus* Cuvier, 1807 (Reptilia: Crocodilia: Alligatoridae). *Journal of Natural History*, *46*, 2979–2984.

Crosby, E. C. (1917). The forebrain of *Alligator mississippiensis*. *Journal of Comparative Neurology*, *27*, 325–402.

Dodson, P. (1975). Functional and ecological significance of relative growth in *alligator*. *Journal of Zoology (London)*, *175*, 315–355.

Farmer, C. G. (2006). On the origin of avian air sacs. *Respiration Physiology and Neurobiology*, *154*, 89–106.

Farmer, C. G. (2015a). The evolution of unidirectional pulmonary airflow. *Physiology*, *30*, 260–272.

Farmer, C. G. (2015b). Similarity of crocodilian and avian lungs indicates unidirectional flow is ancestral for archosaurs. *Integrative and Comparative Biology*, *55*(6), 962–971.

Farmer, C. G. (2015c). Unidirectional flow in lizard lungs: A paradigm shift in our understanding of lung evolution in Diapsida. *Zoology*, *118*, 299–301.

Farmer, C. G. (2021). Linking structure and function in the vertebrate respiratory system: A tribute to August Krogh. *Comparative Biochemistry and Physiology, Part A*, *255*, 110892.

Farmer, C. G., & Sanders, K. (2010). Unidirectional airflow in the lungs of alligators. *Science*, *327*, 338–340.

Gans, C., & Clark, B. (1976). Studies on ventilation of *Caiman crocodilus* (Crocodilia: Reptilia). *Respiration Physiology*, *26*, 285–301.

Hedrick, B. P., Schachner, E. R., & Dodson, P. (2021). Alligator appendicular architecture across an ontogenetic niche shift. *The Anatomical Record*. https://doi.org/10.1002/ar.24717

Holliday, C. M., Tsai, H. P., Skiljan, R. J., George, I. D., & Pathan, S. (2013). A 3D interactive model and atlas of the jaw musculature of *Alligator mississippiensis*. *PLoS One*, *8*, e62806.

Lawson, A. B., Hedrick, B. P., Echols, S., & Schachner, E. R. (2021). Anatomy, variation, and asymmetry of the bronchial tree in the

African grey parrot (*Psittacus erithacus*). *Journal of Anatomy*, *282*, 701–719.

Legendre, P., & Oksanen, M. J.. (2018). Package 'lmodel2'. Retrieved from https://CRAN.R-project.org/package=lmodel2.

Lessner, E. J., & Holliday, C. M. (2020). A 3D ontogenetic atlas of *Alligator mississippiensis* cranial nerves and their significance for comparative neurology of reptiles. *The Anatomical Record*. https://doi.org/10.1002/ar.24550

Locy, W. A., & Larsell, O. (1916a). The embryology of the bird's lung based on observations of the domestic fowl part I. *The American Journal of Anatomy*, *19*, 447–506.

Locy, W. A., & Larsell, O. (1916b). The embryology of the bird's lung based on observations of the domestic fowl part II. *The American Journal of Anatomy*, *20*, 1–44.

Malte, C. L., Malte, H., & Wang, T. (2016). The long road to steady state in gas exchange: Metabolic and ventilatory responses to hypercapnia and hypoxia in Cuvier's dwarf caiman. *Journal of Experimental Biology*, *219*, 3810–3821.

O'Connor, P. M. (2006). Postcranial pneumaticity: An evaluation of soft-tissue influences on the postcranial skeleton and the reconstruction of pulmonary anatomy in archosaurs. *Journal of Morphology*, *267*, 1199–1226.

O'Connor, P. M. (2009). Evolution of the archosaurian body plans: Skeletal adaptations of an air-sac-based breathing apparatus in birds and other archosaurs. *Journal of Experimental Zoology*, *311A*, 629–646.

O'Connor, P. M. O., & Claessens, L. P. A. M. (2005). Basic avian pulmonary design and flow-through ventilation in non-avian theropod dinosaurs. *Nature*, *436*, 253–256.

Oaks, J. R. (2011). A time-calibrated species tree of Crocodylia reveals a recent radiation of the true crocodiles. *Evolution*, *65*, 3285–3297.

Perry, S. F. (1988). Functional morphology of the lungs of the nile crocodile, *Crocodylus niloticus*: Non-respiratory parameters. *Journal of Experimental Biology*, *134*, 99–117.

Radermacher, V. J., Fernandez, V., Schachner, E. R., Butler, R. J., Bordy, E. M., Hudgins, M. N., de Klerk, W. J., Chapelle, K. E. J., & Choiniere, J. N. (2021). A new *Heterodontosaurus* specimen elucidates the unique ventilatory macroevolution of ornithischian dinosaurs. *eLife*, *10*, e66036.

Reichert, M. N., de Oliveira, P. R. C., Souza, G. M. P. R., Moranza, H. G., Restan, W. A. Z., Abe, A. S., Klein, W., & Milsom, W. K. (2019). The respiratory mechanics of the yacare caiman (*Caiman yacare*). *Journal of Experimental Biology*, *222*, jeb193037.

Sanders, R. K., & Farmer, C. G. (2012). The pulmonary anatomy of *Alligator mississippiensis* and its similarity to the avian respiratory system. *The Anatomical Record*, *295*, 699–714.

Scavezzoni, E., & Fischer, V. (2021). The postcranial skeleton of *Cerrejonisuchus improcerus* (Crocodyliformes: Dyrosauridae) and the unusual anatomy of dyrosaurids. *PeerJ*, *9*, e11222.

Schachner, E. R., Farmer, C. G., McDonald, A. T., & Dodson, P. (2011). Evolution of the Dinosauriform respiratory apparatus: New evidence from the postcranial axial skeleton. *The Anatomical Record*, *294*, 1532–1547.

Schachner, E. R., Hedrick, B. P., Richbourg, H. R., Hutchinson, J. R., & Farmer, C. G. (2021). Anatomy, ontogeny, and evolution of the archosaurian respiratory system: A case study on *Alligator mississippiensis* and *Struthio camelus*. *Journal of Anatomy*, *238*, 845–873.

Schachner, E. R., Hutchinson, J. R., & Farmer, C. G. (2013). Pulmonary anatomy in the Nile crocodile and the evolution of unidirectional airflow in Archosauria. *PeerJ*, *1*, e60. https://doi.org/10.7717/peerj.7760

Schachner, E. R., Lyson, T., & Dodson, P. (2009). Evidence from rib and vertebral morphology for the evolution of the avian respiratory system in non-avian theropod dinosaurs. *Anatomical Record*, *292*, 1501–1513.

Schachner, E. R., Sedlmayr, J. C., Schott, R., Lyson, T. R., Sanders, R. K., & Lambertz, M. (2017). Pulmonary anatomy and a case of unilateral aplasia in a common snapping turtle (*Chelydra serpentina*): Developmental perspectives on cryptodiran lungs. *Journal of Anatomy*, *231*, 835–848.

Sereno, P. C., Martinez, R. N., Wilson, J. A., Varricchio, D. J., Alcober, O. A., & Larsson, H. C. E. (2008). Evidence for avian intrathoracic air sacs in a new predatory dinosaur from Argentina. *PLoS One*, *3*, e3303.

Sokal, R. R., & Rohlf, F. J. (2012). *Biometry* (4th ed.). WH Freeman and Company.

Tattersall, G. J., de Andrade, D. V., Brito, S. P., Abe, S. A., & Milsom, W. K. (2006). Regulation of ventilation in the caiman (*Caiman latirostris*): Effects of inspired CO_2 on pulmonary and upper airway chemoreceptors. *Journal of Comparative Physiology B*, *176*, 125–138.

Uriona, T. J., & Farmer, C. G. (2008). Recruitment of the *diaphragmaticus*, *ischiopubis*, and other respiratory muscles to control pitch and roll in the American alligator (*Alligator mississippiensis*). *Journal of Experimental Biology*, *211*, 1141–1147.

Wedel, M. J. (2003). Vertebral pneumaticity, air sacs, and the physiology of sauropod dinosaurs. *Paleobiology*, *29*, 243–255.

Wedel, M. J. (2009). Evidence for bird-like air sacs in saurischian dinosaurs. *Journal of Experimental Zoology*, *311A*, 611–628.

SUPPORTING INFORMATION

Additional supporting information may be found in the online version of the article at the publisher's website.

How to cite this article: Schachner, E. R., Diaz, R. E., Coke, R., Echols, S., Osborn, M. L., & Hedrick, B. P. (2022). Architecture of the bronchial tree in Cuvier's dwarf caiman (*Paleosuchus palpebrosus*). *The Anatomical Record*, 1–18. https://doi.org/10.1002/ar.24919